SCIENTIFIC REPORTS

OPEN

Kinesin-6 Klp9 plays motor-dependent and -independent roles in collaboration with Kinesin-5 Cut7 and the microtubule crosslinker Ase1 in fission yeast

Received: 17 October 2018
Accepted: 1 May 2019
Published online: 14 May 2019

Masashi Yukawa[1,2], Masaki Okazaki[2], Yasuhiro Teratani[2], Ken'ya Furuta[3] & Takashi Toda[1,2]

Bipolar mitotic spindles play a critical part in accurate chromosome segregation. During late mitosis, spindle microtubules undergo drastic elongation in a process called anaphase B. Two kinesin motors, Kinesin-5 and Kinesin-6, are thought to generate outward forces to drive spindle elongation, and the microtubule crosslinker Ase1/PRC1 maintains structural integrity of antiparallel microtubules. However, how these three proteins orchestrate this process remains unknown. Here we explore the functional interplay among fission yeast Kinesin-5/Cut7, Kinesin-6/Klp9 and Ase1. Using total internal reflection fluorescence microscopy, we show that Klp9 forms homotetramers and that Klp9 is a processive plus end-directed motor. *klp9Δase1Δ* is synthetically lethal. Surprisingly, this lethality is not ascribable to the defective motor activity of Klp9; instead, it is dependent upon a nuclear localisation signal and coiled coil domains within the non-motor region. We isolated a *cut7* mutant (*cut7-122*) that displays temperature sensitivity only in the absence of Klp9. Interestingly, *cut7-122* alone is impaired in spindle elongation during anaphase B, and furthermore, *cut7-122klp9Δ* double mutants exhibit additive defects. We propose that Klp9 plays dual roles during anaphase B; one is motor-dependent that collaborates with Cut7 in force generation, while the other is motor-independent that ensures structural integrity of spindle microtubules together with Ase1.

Bipolar spindle assembly is essential for proper sister chromatid segregation. Aberrations in this process result in chromosome missegregation and the emergence of aneuploid progenies, leading to miscarriages, birth defects and several human diseases, including cancer[1,2]. The formation of bipolar spindle microtubules consists of multiple, sequential steps, in which a myriad of proteins, including motor molecules, non-motor microtubule associated proteins (MAPs) and regulatory protein-modifying enzymes, act in a coordinated spatiotemporal manner.

Establishment of spindle bipolarity is driven by separation of duplicated centrosomes (the spindle pole bodies, SPBs, in fungi), in which Kinesin-5 motors play the major role (budding yeast Cin8 and Kip1, fission yeast Cut7, *Aspergillus* BimC, *Drosophila* Klp61F, *Xenopus* Eg5 and human Kif11)[3–9]. Accordingly, in many organisms, Kinesin-5s are essential for cell proliferation; their inactivation results in the formation of lethal monopolar spindles with unseparated centrosomes[10–12]. Kinesin-5s form homotetramers, thereby crosslinking and sliding apart antiparallel microtubules[13,14]. Interestingly, in many systems, outward forces generated by Kinesin-5s are antagonised by opposing inward forces elicited by Kinesin-14 motors; monopolar phenotypes resulting from inactivation of Kinesin-5s are rescued by simultaneous inactivation of Kinesin-14s[15–24]. In fission yeast, temperature sensitive (ts) *cut7* mutations are suppressed by the deletion of either *pkl1* or *klp2* that encodes Kinesin-14[18,19,24–29].

[1]Hiroshima Research Center for Healthy Aging (HiHA), Hiroshima University, 1-3-1 Kagamiyama, Higashi-Hiroshima, 739-8530, Japan. [2]Division of Biological and Life Sciences, Graduate School of Integrated Sciences for Life, Hiroshima University, 1-3-1 Kagamiyama, Higashi-Hiroshima, 739-8530, Japan. [3]Advanced ICT Research Institute, National Institute of Information and Communications Technology, Kobe, Hyogo, 651-2492, Japan. Correspondence and requests for materials should be addressed to M.Y. (email: myukawa@hiroshima-u.ac.jp) or T.T. (email: takashi-toda@hiroshima-u.ac.jp)

Once sister chromatids segregate towards each pole (anaphase A), during which spindle length is kept constant, spindle microtubules resume lengthening (anaphase B), followed by cytokinesis. Anaphase B proceeds through the sliding apart of antiparallel microtubules that generates outward force towards the two centrosomes[30,31]. Except for budding yeast Kinesin-5 members, whether Kinesin-5s are involved in anaphase B spindle elongation *in vivo* is not established. This is partly attributed to the fact that a simple inactivation of Kinesin-5s leads to monopolar spindle formation without reaching anaphase, as this kinesin is required for an initial step in the establishment of spindle bipolarity. Therefore, it is not straightforward to prove the role of this kinesin in later stages of mitosis. In addition, there is another kinesin subfamily that plays a role in spindle elongation specifically during late mitotic stages: that is Kinesin-6[32,33].

Kinesin-6 family members (fission yeast Klp9, *C. elegans* ZEN-4, *Drosophila* Pavarotti and Subito, and human MKLP1/CHO1/Kif23, MKLP2/Kif20A/Rab6-KIFL and MPP1/Kif20B) are localised to the spindle midzone during anaphase B and form homotetramers like Kinesin-5s[34–40]. In higher eukaryotes that possess multiple Kinesin-6 members (eg. human beings and fly), each member makes a distinct contribution to anaphase B spindle elongation and/or cytokinesis in a both independent and cooperative manner[35,41–44]. By contrast, in fission yeast, the sole member of Kinesin-6, Klp9, appears to play multiple roles on its own[26,37,45]. Despite these similarities and adaptations, some evolutionary diversifications exist; for instance, MKLP1/CHO1/Kif23, but not Klp9, is a structural component of the Centralspindlin complex[46].

Another crucial factor for anaphase B spindle elongation is the microtubule crosslinker PRC1/Ase1, which bundles antiparallel microtubules and ensures structural integrity of the spindle midzone[47–51]. Whether Kinesin-5 or Kinesin-6 molecules play any role in microtubule bundling like PRC1/Ase1 *in vivo* independent of their motor activities remains unknown, though it is known that the non-motor domain of Eg5 is required for microtubule crosslinking *in vitro*[52].

We and others previously implicated that Klp9 executes essential functions for cell viability in a redundant fashion with Ase1[25,26,37,45]; however, it is not understood as to how this kinesin functionally collaborates with Ase1. In addition, it has not been firmly established whether Cut7 acts in spindle elongation during late mitosis on its own as well as in early mitosis, and furthermore the functional interplay between Cut7 and Klp9 remains to be determined[25,26]. In this study, we address the following three specific questions. First, is Klp9 indeed a plus-end motor and if so, how does it behave *in vitro*? Second, how do Klp9 and Ase1 collaborate in spindle integrity during anaphase B? Lastly, does Cut7 drive spindle elongation during anaphase B as a motor in accordance with Klp9? We show that Klp9 plays a microtubule-crosslinking role that is independent of plus end-directed motility and that Cut7 drives spindle elongation during anaphase B. Consequently, we can draw a detailed picture of the molecular interplays between two mitotic kinesins and the microtubule crosslinker during late mitotic stages.

Results

Klp9 forms homotetramers. Klp9 belongs to the kinesin-6 family, yet its biophysical characterisation with regards to motor activity has not been reported. In addition, whether Klp9 forms homodimers or homotetramers has not been clarified[37]. Therefore, as a first step, we expressed and purified recombinant full-length Klp9 protein tagged with EGFP (Klp9-EGFP) (Supplementary Fig. S1). To assess the oligomeric state of Klp9, we imaged the fluorescence spots of single Klp9-EGFP molecules adsorbed onto a glass surface. Although some spots showed two-step photobleaching behaviour, importantly, a population of spots displayed photobleaching in more than two steps (Fig. 1A), suggesting that Klp9-EGFP molecules form homotetramers.

We then quantified the intensities of the Klp9-EGFP spots and compared them with those of well-characterised dimeric kinesin-1-EGFP and tetrameric Eg5-EGFP[53] (Fig. 1B). The intensity profile of Klp9-EGFP is clearly more similar to that of tetrameric Eg5-EGFP than dimeric kinesin-1-EGFP, confirming that Klp9 is tetrameric.

Klp9 is a plus end-directed processive motor. To examine the motor activity of Klp9, we performed *in vitro* assay with total internal reflection fluorescence microscopy (TIRFM). Purified Klp9 was immobilised onto a glass surface via an anti-His antibody, followed by the addition of paclitaxel (taxol)-stabilised, polarity-marked microtubules (Fig. 1C). This microtubule gliding assay showed that Klp9 could translocate microtubules with the minus end leading at a velocity of 39.0 ± 0.3 nm/s ($n = 96$, $N = 3$) (Fig. 1D,E), indicating that Klp9 moved towards the microtubule plus ends.

Next, we added purified Klp9-EGFP proteins to immobilised, polarity-marked microtubules at a concentration of 0.3 nM and observed the behaviour of Klp9 at the single molecule level on the microtubule (Fig. 1F). As shown in Fig. 1G, Klp9 displayed processive motility toward the plus ends of microtubules. Quantification of Klp9 motility showed that Klp9 walked on the microtubule with a velocity of 21 ± 2 nm/s (Fig. 1H; $n = 216$, $N = 3$) and its average run length was 430 ± 29 nm (Fig. 1I). These *in vitro* results firmly establish that Klp9 is a processive motor with plus end-directed motility.

The Klp9 motor is an important determinant for spindle elongation rate during anaphase B. We previously isolated a *klp9* ts mutant that contains a missense mutation within the N-terminal motor domain (*klp9-2*, K333M)[26]. In addition, an ATPase-defective *klp9* rigor mutant containing a point mutation in the switch II region within the motor domain (*Klp9*^{rigor}, G296A) was previously constructed[45]. We examined Klp9 localisation (tagged with YFP under the native promotor) in these mutants and compared it with wild type Klp9 (a microtubule was simultaneously visualised with mCherry-Atb2 (α2-tubulin)[54]). Interestingly, while Klp9-YFP concentrated on the middle region of spindle microtubules during anaphase B, corresponding to the spindle midzone in which antiparallel microtubules overlap[37], both Klp9-2-YFP and Klp9^{rigor}-YFP were localised along spindle microtubules in a more diffuse manner (Fig. 2A,B). These localisation patterns are consistent with the notion that Klp9 possesses a plus-end motility, thereby accumulating on the spindle midzone.

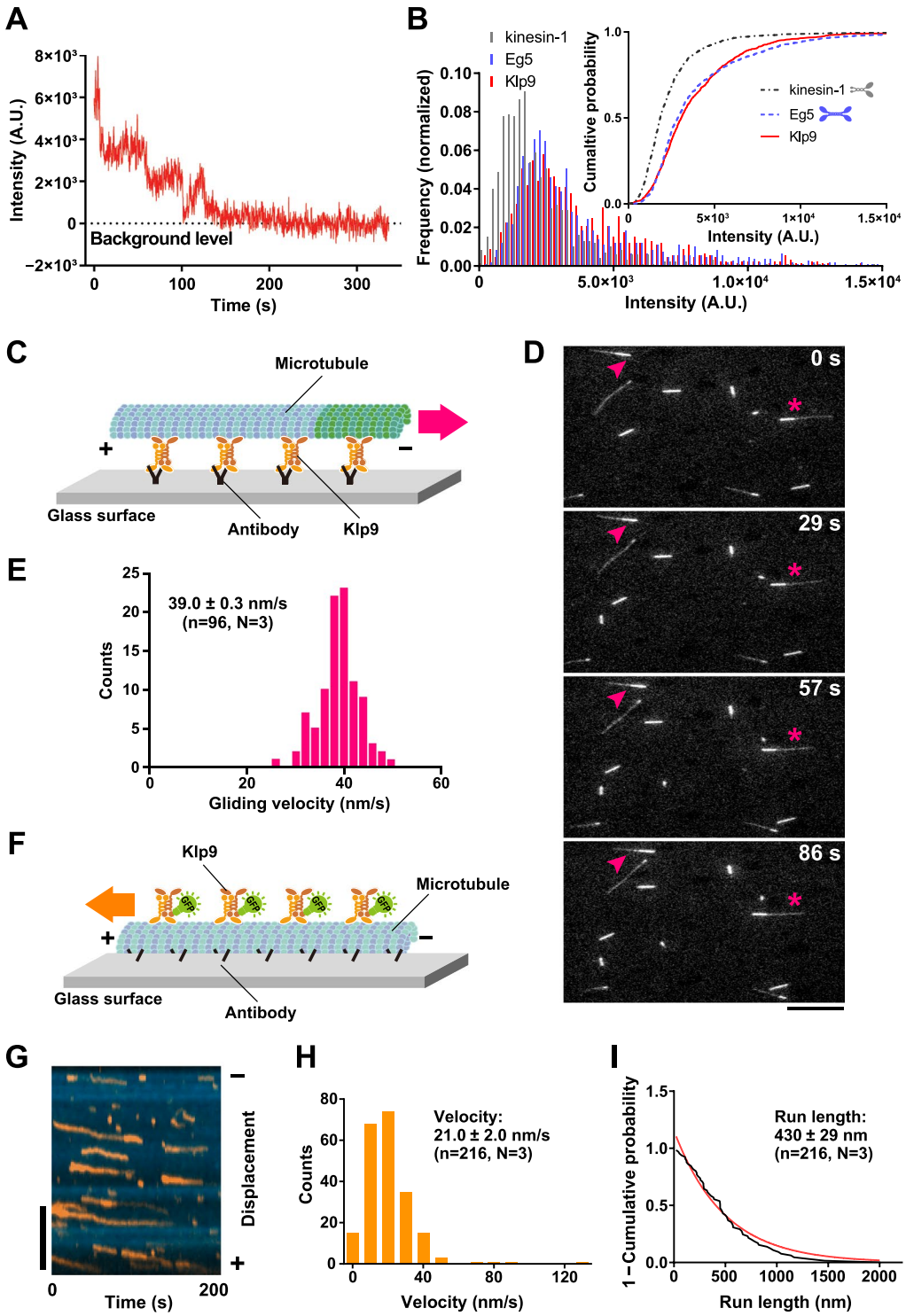

Figure 1. Klp9 is a processive plus end-directed motor. (**A**) Photobleaching behaviour of a surface-bound spot of full-length Klp9-EGFP. (**B**) Histograms of initial intensities of surface-bound Klp9-EGFP (n = 933), dimeric kinesin-1-EGFP (n = 1007) and tetrameric Eg5-EGFP (n = 1111). The histograms were normalised by dividing the individual bins by the total number of fluorescence spots analysed. The upper-right inset shows cumulative probability of the same data. (**C**) Scheme of the *in vitro* microtubule gliding assay. (**D**) Representative time lapse images of the microtubule gliding assay. Paclitaxel-stabilised, polarity-marked microtubules were added to slides coated with purified full-length Klp9 proteins in the presence of 1 mM ATP. Microtubule gliding was viewed by TIRFM. Images were taken every 1 s, and the time in the panels, in seconds, is shown on the top right. Two microtubule ends moving towards the minus ends are shown with arrowheads and asterisks. Scale bar, 10 μm. (**E**) Distribution and the average value of gliding velocity. (**F**) Scheme of the single-molecule assay. (**G**) Processive motility of single full-length Klp9-EGFP molecules towards the plus end of paclitaxel-stabilised microtubules. Representative TIRFM kymograph depicting the movement of 0.3 nM Klp9-EGFP

(orange) on a microtubule (blue) in the presence of 1 mM ATP is shown. Scale bar, 5 μm. (**H**,**I**) Velocity histogram (**H**) and cumulative probability (**I**) of single Klp9-EGFP molecules. The average value and the standard error of the mean values from the three independent experiments are shown (n = 50, 101 and 65). The mean run length value for each experiment was obtained by fitting each data set to 1−cumulative probability, $Y = 1 - [1 - \exp\{(X_0 - X)/\lambda\}]$, where λ represents the mean run length.

We then measured spindle elongation rate in these mutants as well as in a *klp9* deletion strain (*klp9Δ*). In all three mutants examined, spindle elongation rate was significantly reduced compared with wild type cells (~50% reduction, 0.75 ± 0.09 for wild type vs 0.38 ± 0.09–0.43 ± 0.06 for the three *klp9* mutants, Fig. 2C,D). By contrast, we did not detect any delay regarding anaphase onset in either *klp9*^{rigor} or *klp9-2* cells (Fig. 2E). It is of note that, a modest, yet significant delay was observed in *klp9Δ* cells, consistent with a previous report[45]. This is attributable to a motor-independent role of Klp9 in controlling the timing of anaphase onset (Fig. 2E). Overall, these results indicate that Klp9 is a plus-end motor that is crucial for determining the rate of anaphase B spindle elongation.

Klp9 plays an additional role during anaphase B independent of its motor activity in collaboration with the microtubule crosslinker Ase1. Ase1 is a homologue of vertebrate PRC1 and plays a vital role in spindle assembly and stability as an antiparallel microtubule bundler/crosslinker[49–51,55]. Previous work showed that a *klp9Δase1Δ* double deletion strain is inviable[37], which we also found (Fig. 3A top). However, it is not established as to how these two MAPs functionally interact and ensure cell viability in collaboration[25,37,45]. As Klp9 is a plus end-directed motor, the simplest scenario would be that Ase1-mediated microtubule crosslinking and Klp9 motor-dependent microtubule sliding activities are required for spindle integrity in a functionally redundant fashion. To interrogate this possibility, we crossed *ase1Δ* with the motor-defective *klp9-2*. Intriguingly and rather unexpectedly, we found that the resulting *klp9-2ase1*Δ double mutant strain was not ts (Fig. 3B). In sharp contrast, *cut7*Δ*pkl1*Δ double mutants that require motor activity of Klp9 for survival[26] displayed ts lethality in combination with *klp9-2* (Fig. 3B). This result implies that Klp9 motor activity alone does not confer viability of *ase1*Δ cells.

To substantiate this notion, we crossed *klp9*^{rigor} with *ase1Δ* and found that the double mutant was indeed viable and capable of forming colonies at any temperatures including 36 °C (Fig. 3A, bottom and 3B). This indicates that defective motor activity of Klp9 is not responsible for synthetic lethality between *ase1*Δ and *klp9*Δ. In order to decipher the essential role of Klp9 in the absence of Ase1, we next investigated the functional domain within Klp9 that is required for viability of *ase1Δ* cells.

Systematic truncation and mutation analysis of Klp9 highlights the importance of a nuclear localisation signal in the C-terminal non-motor region. It was reported that Klp9 plays one additional, motor-independent role in regulating the timing of anaphase onset (see Fig. 2E), which requires the C-terminal 38 amino acid residues[45]. Crossing *ase1*Δ with the *klp9* mutant lacking this region (*klp9-Δ38C*) showed that the double mutant was still viable (Fig. 4A and Supplementary Fig. S2A), indicating that the role of Klp9 in anaphase onset is not involved in the functional redundancy with Ase1. We then systematically created a series of C-terminally truncated *klp9* mutants at the endogenous locus under the native promotor with GFP in the C-terminus, and crossed them with *ase1*Δ. These included Klp9-Δ92C, Klp9-Δ133C and Klp9-Δ172C, the latter two which lack one of the two coiled coil domains and Klp9-Δ234C that does not contain either of coiled coil domains (Fig. 4A) and finally, Klp9-ΔMotor that consists of only the C-terminal non-motor domain. It was found that all the truncation mutants except for *klp9-Δ38C* were synthetically lethal with *ase1*Δ (Fig. 4A and Supplementary Fig. S2B,C).

We also observed the cellular localisation of individual Klp9 mutants during interphase and mitosis. Previous work showed that full-length Klp9 is localised to the nucleus throughout the cell cycle, but its localisation pattern differs depending upon cell cycle stages; it occupies the entire nucleoplasm from interphase until mid-mitosis, and then translocates to the spindle midzone in late mitosis[37]. First, we confirmed this profile (Fig. 4A,B). Interestingly, Klp9-Δ92C, but not Klp9-Δ38C or Klp9-ΔMotor, lost nucleoplasmic localisation during interphase. We noted that the mitotic localisation of Klp9-Δ92C to the spindle midzone was somehow still retained (Fig. 4A,B), though precise quantification of signal intensities showed a substantial reduction compared to those in wild type cells (Fig. 4C). By contrast, all the other truncation mutants (Klp9-Δ133C, -Δ172C, -Δ234C) did not localise to either the nucleus or the spindle midzone (Fig. 4A–C). We then measured spindle elongation rate of each mutant during anaphase B. As shown in Fig. 4E, all mutants showed compromised spindle elongation during late mitosis (Fig. 4E).

Nuclear localisation of Klp9 during interphase suggested the presence of a nuclear localisation signal (NLS)[56]. Computational search picked up a putative NLS between 546th and 578th that contains three consecutive basic amino acids (573K-574R-575K, Fig. 4D). The replacement of three basic residues with alanines (designated Klp9-KARAKA) abolished the nuclear localisation during interphase despite that Klp9-KARAKA was capable of weakly localising to the anaphase B spindle like Klp9-Δ92C (Fig. 4A–C). Importantly, *klp9-KARAKA* was synthetically lethal with *ase1*Δ (Fig. 4A,B and Supplementary Fig. S2B,C); thus *klp9-KARAKA* recapitulated defective profiles of *klp9-Δ92C*. It should be noted that all the mutants created, except for *klp9-Δ38C*, also exhibited synthetic lethality in combination with *cut7*Δ*pkl1*Δ (Supplementary Fig. S2A,C). Collectively, the domain analysis shown here has unveiled the existence of the NLS that is essential for correct localisation and function of Klp9.

Two internal coiled coil regions are crucial for Klp9 function in collaboration with Ase1. Next, we created internal deletion mutants of Klp9. The C-terminal region of Klp9 contains two coiled coil domains (CC1, 421–461 and CC2, 501–541). We deleted each region and integrated it into the endogenous locus with GFP in the C-terminus (designated Klp9-ΔCC1 and Klp9-ΔCC2 respectively) (Fig. 5A). The cellular localisation of

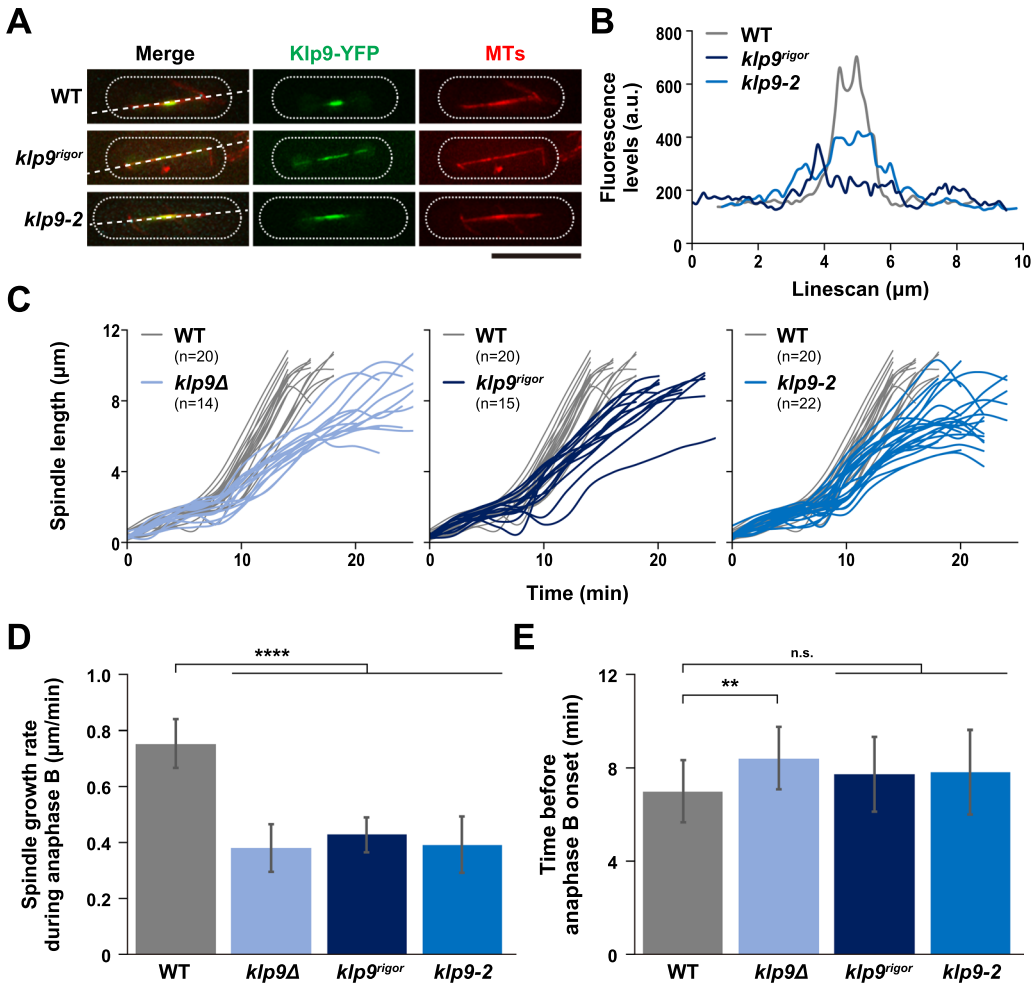

Figure 2. The Klp9 motor is an important determinant for spindle elongation rate during anaphase B. (**A**) Klp9-YFP becomes dispersed along the mitotic spindle in the *klp9* motor mutants. Representative images showing mitotic localisation of Klp9-YFP in the indicated strains are presented. Cells of wild type, *klp9*^{rigor} and *klp9-2* (carrying Klp9-YFP and mCherry-Atb2) were shifted from 27 °C to 36 °C, and incubated for 2 h. Scale bar, 10 μm. Lines used for quantification of Klp9-YFP signals in (**B**) are shown on the left panels. (**B**) Representative line scans of Klp9-YFP in wild type (grey line), *klp9*^{rigor} (dark blue line) and *klp9-2* (blue line) taken along the spindle axis and between the two SPBs (dotted lines) as shown in (**A**). (**C**) Profiles of mitotic progression in *klp9*Δ (light blue line, n = 14), *klp9*^{rigor} (dark blue line, n = 15) or *klp9-2* cells (blue line, n = 22). Each strain contains a tubulin marker (mCherry-Atb2) and an SPB marker (Cut12-GFP). Cells were grown at 36 °C for 4 h and live imaging performed thereafter. Changes of the inter-SPB distance were plotted against time. In each panel, patterns of wild type cells are plotted for comparison (grey line, n = 20). (**D**) Spindle growth rate during anaphase B. (**E**) The time between the initiation of SPB separation and onset of anaphase B. Data are given as means ± SD; $^{**}P < 0.01$; $^{****}P < 0.0001$; n.s., not significant (two-tailed unpaired Student's *t*-test).

these Klp9 mutants showed that neither of them was localised to the spindle midzone in late mitosis (Fig. 5B,C). It is noteworthy that interphase nuclear localisation was retained in these mutants, consistent with the notion that they contain the C-terminal NLS identified earlier (see Fig. 4). Genetic analysis indicated that both deletion mutants were synthetically lethal with either *ase1*Δ or *cut7*Δ*pkl1*Δ (Fig. 5D and Supplementary Fig. S2A,C), implying that both CC1 and CC2 are indispensable for Klp9 function. We also measured spindle elongation rate during anaphase B in these deletion mutants, and found that each exhibited the decrease of spindle growth rate (Fig. 5E). It is worth noting that plotting spindle elongation rate against fluorescence intensities of individual mutants including truncation mutants analysed earlier (Fig. 4C,E) and coiled coil mutants (Δ*CC1* and Δ*CC2*, Fig. 5C,E) indicate a proportional linear relationship: cells displaying more intense Klp9-GFP signals on spindle midzone elongate faster during anaphase B (Fig. 5F), which is consistent with results recently reported[57]. Taken together, these results highlight that the C-terminal coiled coil domains are essential for Klp9's plus end-directed motor activity as well as its motor-independent role in cooperation with Ase1.

Kinesin-5 Cut7 collaborates with Klp9 in spindle elongation during anaphase B. In *klp9* mutants with defects in motor activity (eg. Klp9-2 and Klp9^{rigor}), spindle elongation during anaphase B was substantially

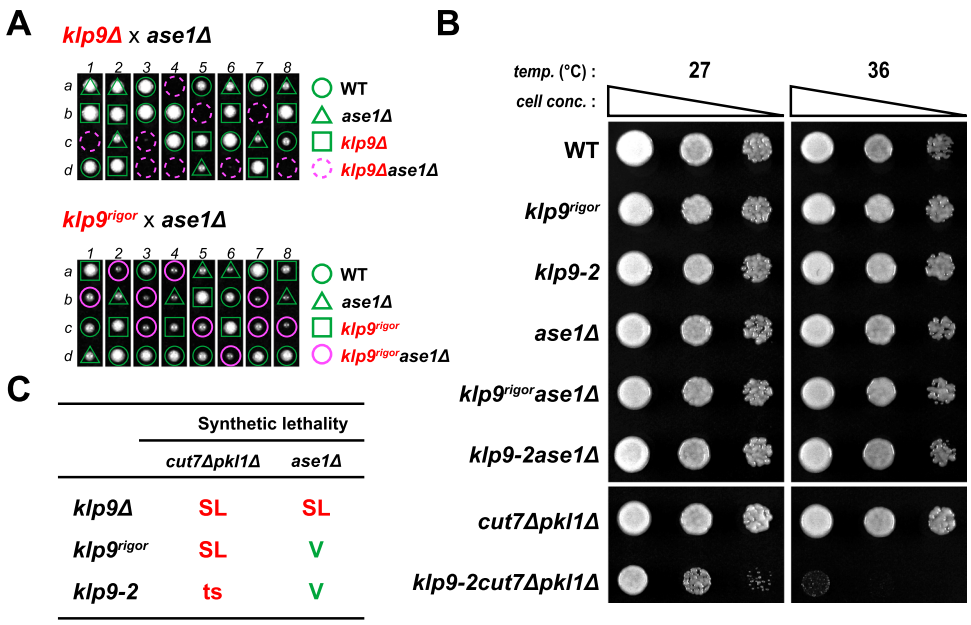

C

	Synthetic lethality	
	cut7Δpkl1Δ	*ase1Δ*
klp9Δ	SL	SL
klp9rigor	SL	V
klp9-2	ts	V

Figure 3. Klp9 plays an additional role during anaphase B independent of its motor activity in collaboration with Ase1. (**A**) Tetrad analysis. Spores were dissected upon crosses between *klp9*Δ and *ase1*Δ strains (top) or between *klp9*^{rigor} and *ase1*Δ strains (bottom), respectively. Individual spores (a–d) in each ascus (1–8) were dissected on YE5S plates and incubated for 3 d at 27 °C. Representative tetrad patterns are shown. Circles, triangles and squares with green lines indicate wild type, *ase1*Δ single mutants and *klp9* single mutants, respectively. Assuming 2:2 segregation of individual markers allows the identification of lethal *klp9*Δ*ase1*Δ double mutants (indicated by dashed magenta circles). Circles with magenta lines indicate *klp9*^{rigor}*ase1*Δ double mutants. (**B**) Spot test. Indicated strains were serially (10-fold) diluted, spotted onto rich YE5S plates and incubated at 27 °C or 36 °C for 2 d. *cell conc*., cell concentration, *temp*., temperature. (**C**) Summary of genetic interactions between the *klp9* mutants (*klp9*Δ, *klp9*^{rigor} or *klp9-2*) and *cut7*Δ*pkl1*Δ or between the *klp9* mutants and *ase1*Δ. SL, synthetic lethal. V, viable. ts, temperature sensitive.

compromised; however, spindles were still capable of elongating, albeit with a reduced rate (see Fig. 2C,D). Previous studies suggested the contribution of Cut7 in late mitosis[25,26,58]. However, there is no direct evidence for the requirement of Cut7 in anaphase B spindle elongation and this issue remains under debate[37]. One of the reasons for this conundrum is that Cut7 is required in the early stages of spindle assembly. As defects in SPB separation leads to the formation of monopolar spindles at restrictive temperatures, all available *cut7* ts mutants do not reach anaphase B[5,18,58]. We posited that if Cut7 is also involved in a later step of spindle assembly, a novel type of conditional mutants could be isolated, in which they are defective only during late mitosis and exhibit the ts phenotype only in the background of *klp9*Δ; in other words, such *cut7* mutants would not be ts for growth on their own.

Given this assumption, we introduced PCR-mutagenised *cut7* fragments into *klp9*Δ cells and screened for ts transformants (see Materials and Methods for details). We then backcrossed individual ts isolates with wild type cells and examined how the ts phenotype segregated in progenies; expected *cut7* mutants should only display temperature sensitivity in the background of *klp9*Δ. A number of anticipated ts mutants were successfully identified (details will be reported elsewhere). In this study, we present one representative mutant called *cut7-122*. As shown in Fig. 6A, *cut7-122* cells displayed the ts phenotype only in the *klp9*Δ background, but not in the presence of Klp9. Nucleotide sequencing of the *cut7-122 ORF* identified two point mutations, which led to amino acid replacements at 134th and 290th residues (M134T and T290K) within the N-terminal motor domain (Fig. 6B).

To study the impact of the *cut7-122* mutant on mitotic spindle elongation on its own or in combination with *klp9*Δ, we observed the dynamic behaviour of spindle microtubules in *cut7-122* or *cut7-122klp9*Δ cells expressing mCherry-Atb2 (a microtubule marker)[54] and Sid4-mRFP (an SPB marker)[59]. Intriguingly, elongation rate of anaphase B spindles was decreased in a single *cut7-122* mutant: 0.67 ± 0.11 μm/min and 0.75 ± 0.09 μm/min for *cut7-122* and wild type cells respectively. Furthermore, *cut7-122klp9*Δ double mutants displayed a very low rate of spindle elongation (0.20 ± 0.06 μm/min, Fig. 6C–E); Cut7 and Klp9 contributed additively to the elongation of anaphase B spindles. It is worth pointing out that a single *cut7-122* mutant did not display a significant delay in anaphase onset (Fig. 6F) unlike previously isolated conventional *cut7* alleles[5,25,26,60]. Note that the measurement of spindle elongation rate during the period prior to anaphase B indicated a modest decrease in *cut7-122* cells compared to wild type cells (0.33 ± 0.09 for wild type vs 0.25 ± 0.06 for *cut7-122*, Supplementary Fig. S3). This sustains the notion that the major, if not sole, defect in this novel *cut7* allele lies in the late stage of mitosis.

Given the synthetic temperature sensitivity between *cut7-122* and *klp9*Δ, we next asked which activity of Klp9 is required for this genetic interaction. We found that *cut7-122* displays the ts phenotype in combination with *klp9*^{rigor}, which is in stark contrast to the result that *cut7-122* did not exhibit the ts growth in combination with

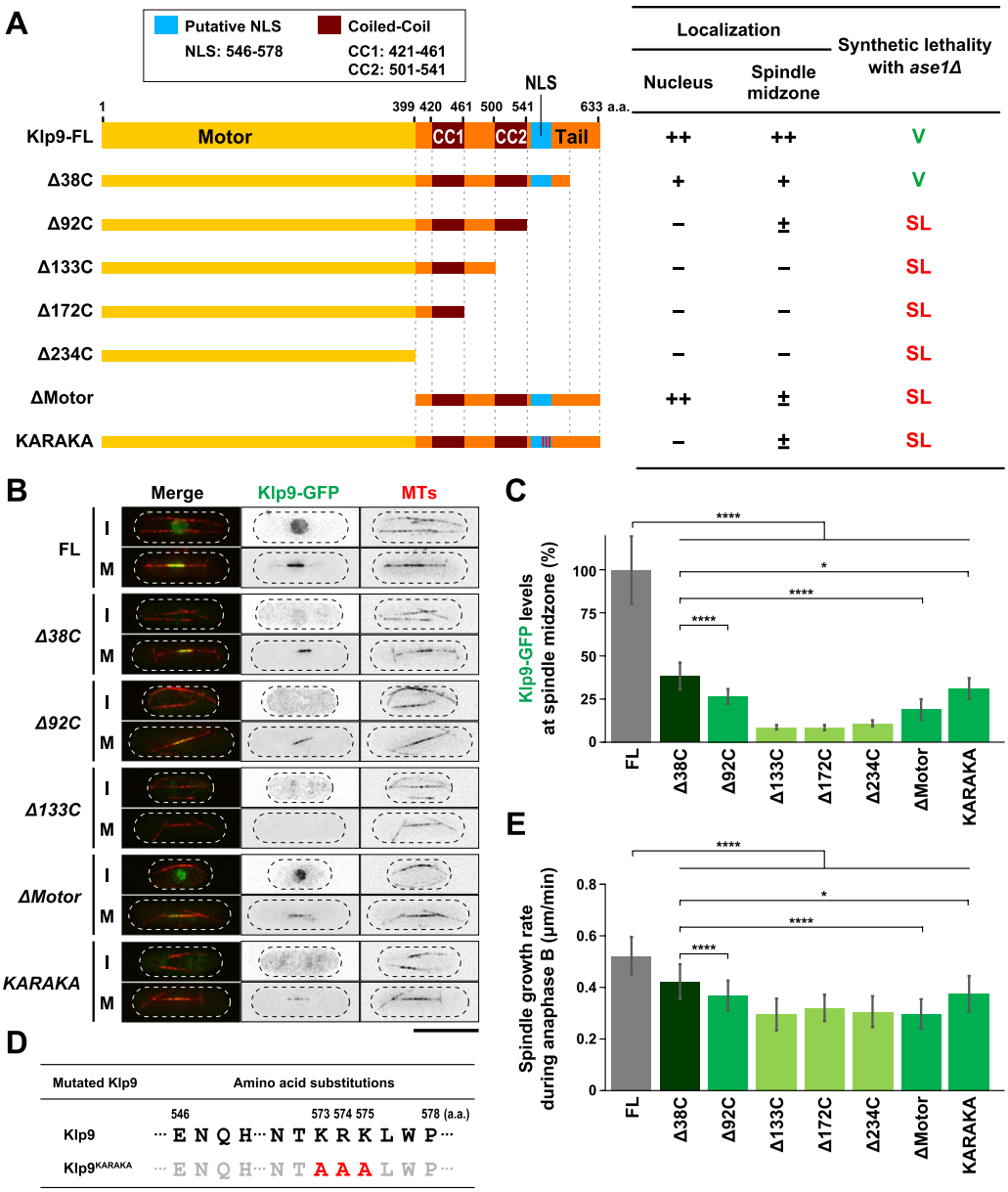

Figure 4. Systematic truncation and mutation analysis of Klp9 highlights the importance of NLS in the C-terminal non-motor region. (**A**) Schematic representation of full-length Klp9 (Klp9-FL), C-terminal truncation mutants (Δ38C, Δ92C, Δ133C, Δ172C and Δ234C), an NLS mutant (KARAKA) and N-terminal truncation mutant (ΔMotor). The table on the right indicates a summary of the cellular localisation and the synthetic lethality of each *klp9* mutant. ++, +, ± and − indicate normal, low, very low and invisible levels of Klp9-GFP localisation in the nucleus or the spindle midzone, respectively. SL, synthetic lethal. V, viable. (**B**) Representative images showing Klp9-GFP localisation during interphase (I) and mitosis (M) in the indicated strains are presented. Scale bar, 10 μm. (**C**) Quantification of Klp9-GFP levels at the midzone of spindle microtubules during anaphase B. Data are given as means ± SD; *P < 0.05; ****P < 0.0001 (two-tailed unpaired Student's *t*-test). (**D**) Substituted amino acid residues in *klp9*^{KARAKA} mutant. These point mutations (K573AR574AK575A) were introduced upon site-directed mutagenesis and confirmed by nucleotide sequencing of the *klp9* gene on the selected clone. (**E**) Spindle growth rate during anaphase B. Data are given as means ± SD; *P < 0.05; ****P < 0.0001 (two-tailed unpaired Student's *t*-test).

*ase1*Δ (Fig. 6A,G). Therefore, the survival of *cut7-122* at the restrictive temperature depends upon the motor activity of Klp9. The profiles of genetic interactions obtained for *klp9*^{rigor}/*klp9-2* and *cut7-122* are identical with regards to Ase1 (Figs 3C and 6G). Thus, we conclude that Cut7 functions in late mitosis as well as early mitosis; it acts in concert with the motor activity of Klp9 in spindle elongation during anaphase B.

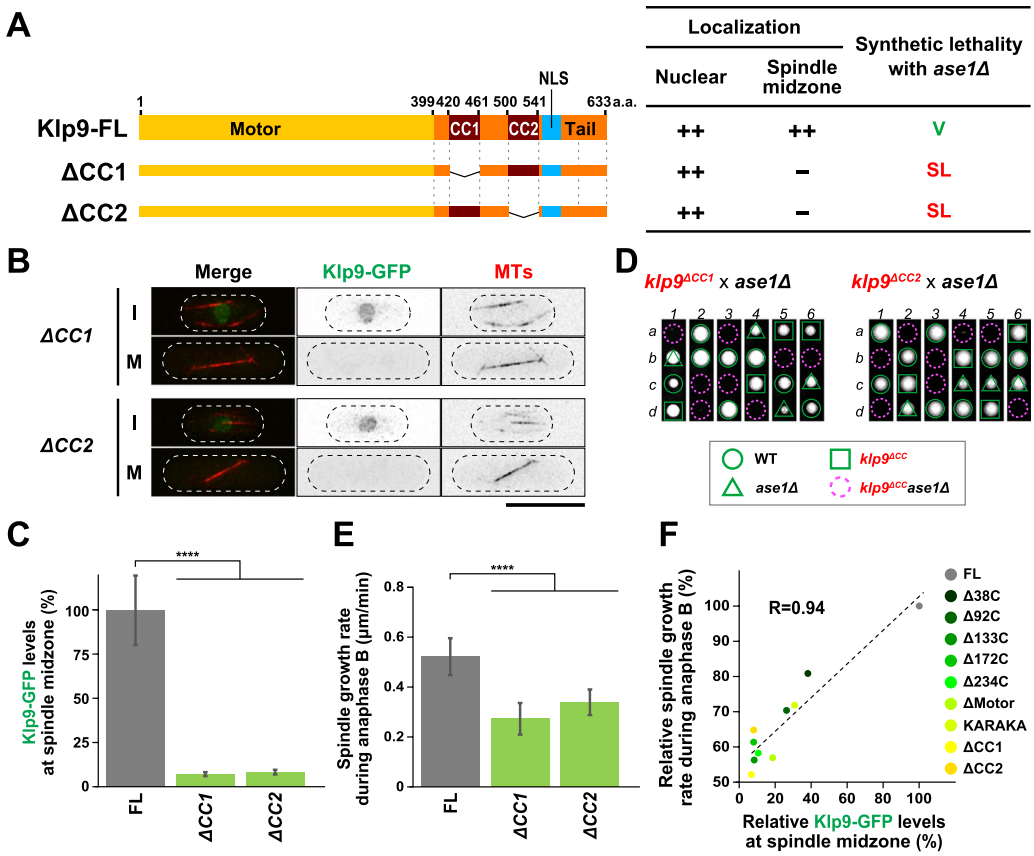

Figure 5. Two internal coiled coil regions are crucial for Klp9 function in collaboration with Ase1. (**A**) Schematic representation of full-length Klp9 (Klp9-FL) and two internal deletion mutants. Each of coiled coil domains (Klp9-ΔCC1: Δ421-461 and Klp9-ΔCC2: Δ501-541) is deleted. The table on the right indicates a summary of the cellular localisation and the synthetic lethality of each *klp9* mutant. ++ and − indicate normal and invisible levels of Klp9-GFP localisation in the nucleus or the spindle midzone, respectively. SL, synthetic lethal. V, viable. (**B**) Representative images showing Klp9-GFP localisation in the indicated strains during interphase (I) and mitosis (M) are presented. Scale bar, 10 μm. (**C**) Quantification of Klp9-GFP levels at the midzone of spindle microtubules during anaphase B. Data are given as means ± SD; ****$P < 0.0001$ (two-tailed unpaired Student's *t*-test). (**D**) Tetrad analysis. Spores were dissected upon crosses between $klp9^{\Delta CC1}$ and *ase1*Δ strains or between $klp9^{\Delta CC2}$ and *ase1*Δ strains respectively. Individual spores (a–d) in each ascus (1–6) were dissected on YE5S plates and incubated for 3 d at 27 °C. Representative tetrad patterns are shown. Circles, triangles and squares with green lines indicate wild type, *ase1*Δ single mutants and $klp9^{\Delta CC}$ single mutants, respectively. Assuming 2:2 segregation of individual markers allows the identification of lethal $klp9^{\Delta CC}$*ase1*Δ double mutants (indicated by dashed magenta circles). (**E**) Spindle growth rate during anaphase B. Data are given as means ± SD; ****$P < 0.0001$ (two-tailed unpaired Student's *t*-test). (**F**) A positive correlation between Klp9 localisation on spindle midzone and spindle elongation rate. Data shown in Figs 4E,F and 5C,E are plotted with regards to spindle growth rate (the vertical axis) and Klp9-GFP fluorescence intensities (the horizontal axis).

Discussion

In this study, we explored the molecular mechanisms by which mitotic spindles elongate during anaphase B in fission yeast. Previous work showed the importance of Kinesin-6 Klp9 and the microtubule crosslinker Ase1[26,37,45]; however, the molecular details underlying the functional interplay between these two MAPs are not known. In addition, it is undetermined whether Kinesin-5 Cut7 on its own plays any role in late mitosis[25,26]. Using biophysical approaches, we show that Klp9 forms homotetramers and is a processive motor with plus-end directionality. Genetic and cell biological analyses indicate that Klp9 collaborates with both Ase1 and Cut7 during anaphase B in two distinct manners. The collaboration with Ase1 is independent of Klp9 motor activity, while the role in combination with Cut7 relies on outward force generated by Klp9 as a motor. Furthermore, isolation of a novel *cut7* mutant allele that is defective in anaphase B spindle elongation has solidified the notion that the Cut7 motor is indeed required for spindle elongation, not only in an early mitotic stage, but also in a later step as well (a model illustrated in Fig. 7).

Kinesin-6 Klp9 is a processive plus end-directed motor. Our *in vitro* assays including photobleaching and fluorescence intensity measurement of Klp9-EGFP indicate that Klp9 forms homotetramers (Fig. 1A,B). Furthermore, TIRFM assay explicitly shows that Klp9 moves towards microtubule plus ends in a processive manner (Fig. 1G,H). The measured velocity of 21 nm/s is comparable with values reported for plus end-directed Kinesin-5 motors[61–63].

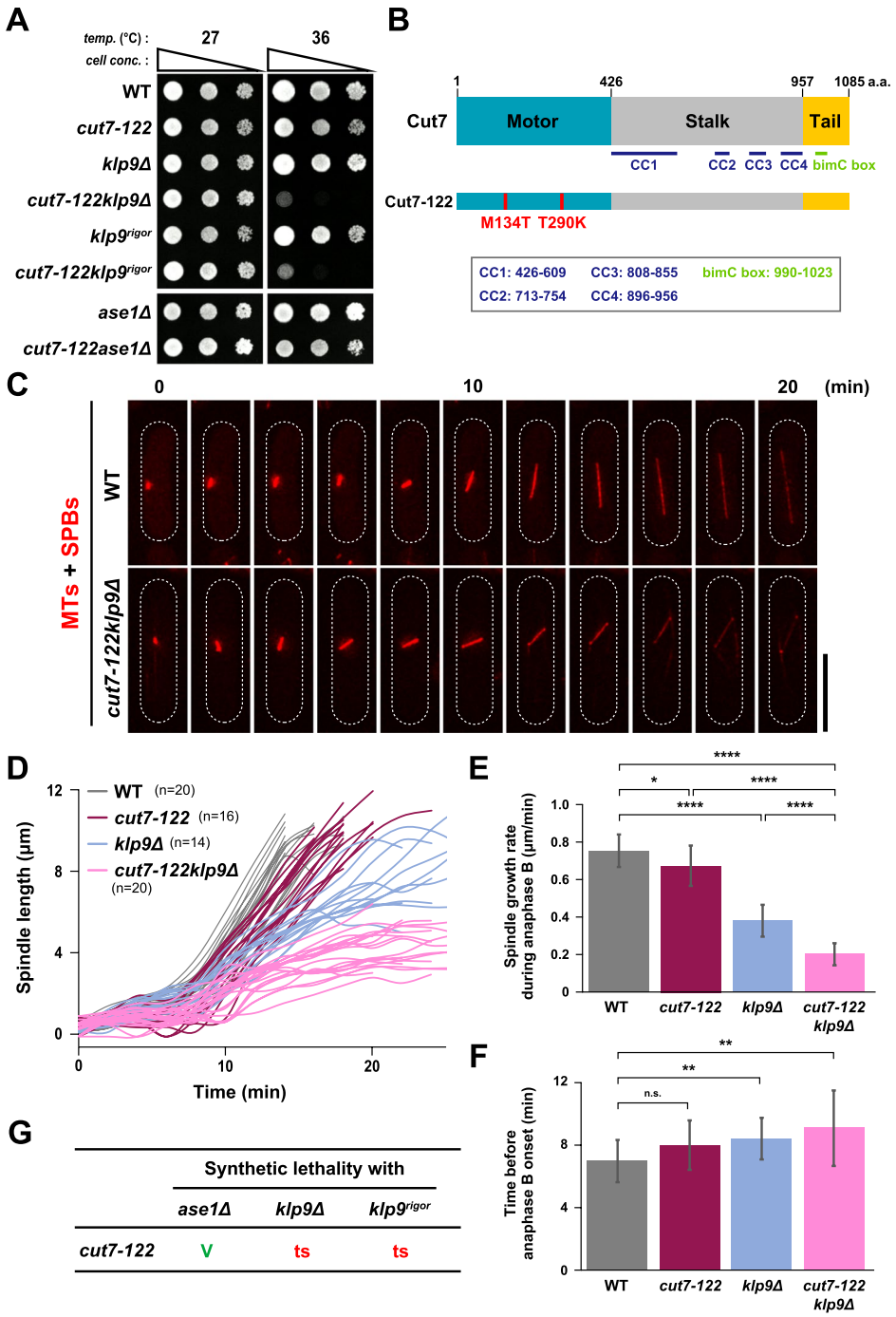

Figure 6. Kinesin-5 Cut7 collaborates with Klp9 in spindle elongation during anaphase B. (**A**) Spot test. Indicated strains were serially (10-fold) diluted, spotted onto rich YE5S plates and incubated at 27 °C or 36 °C for 2 d. *cell conc.*, cell concentration, *temp.*, temperature. (**B**) Mutation sites in the *cut7-122* mutant. Cut7-122 contained two mutations (M134T and T290K) in the C-terminal motor domain. (**C**) Time-lapse images of mitotic wild type and *cut7-122klp9Δ* cells. Spindle microtubules (mCherry-Atb2; red) were visualised. Images were taken at 2 min intervals after incubation of cultures at 36 °C for 4 h. The cell peripheries are outlined with dotted lines. Scale bar, 10 μm. (**D**) Profiles of mitotic progression in *cut7-122* (dark magenta line, n = 16) or *cut7-122klp9Δ* cells (light magenta line, n = 20). Each strain contains a tubulin marker (mCherry-Atb2). Cells were grown at 36 °C for 4 h and live imaging performed thereafter. Changes of the inter-SPB distance were plotted against time. Data for wild type (grey line, n = 20) and *klp9Δ* (light blue line, n = 14) are plotted for comparison and these are the same as those presented in Fig. 2C. (**E**) Spindle growth rate during anaphase B. (**F**) The time between the initiation of SPB separation and onset of anaphase B. Data for wild type and *klp9Δ* are shown for comparison; these are the same as those presented in Fig. 2D,E. Data are given as means ± SD; *P < 0.05; **P < 0.01; ****P < 0.0001; n.s., not significant (two-tailed unpaired Student's *t*-test). (**G**) Summary of genetic interactions between *cut7-122* and *klp9* mutants or *ase1Δ*. V, viable. ts, temperature sensitive.

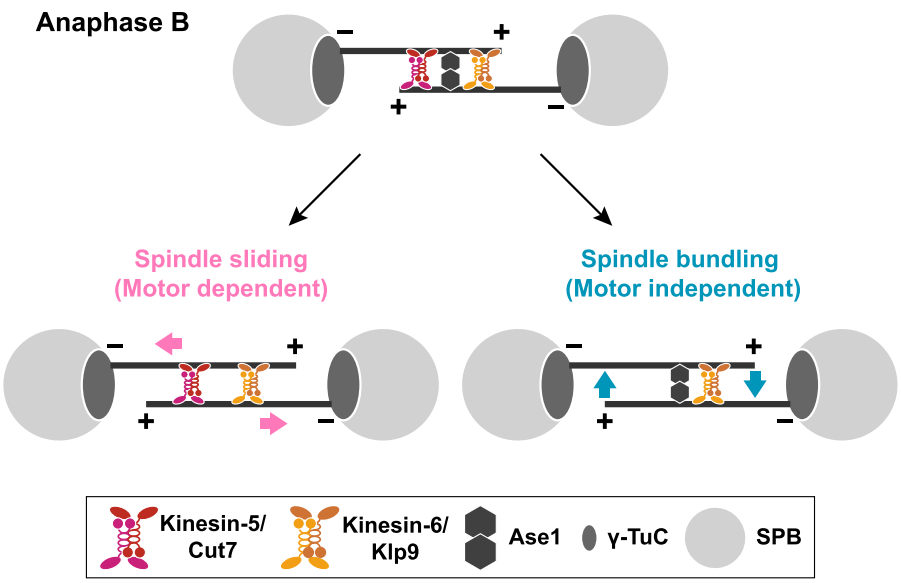

Figure 7. A model of spindle elongation during anaphase B. Spindle elongation during late mitosis is executed by three MAPs, Kinesin-6 Klp9, Kinesin-5 Cut7 and the microtubule crosslinker Ase1. Klp9 plays dual roles in this process; one is motor-dependent and the other is motor-independent. Klp9 motor activity generates outward force, thereby inducing the sliding away of antiparallel microtubules at the spindle midzone (bottom left). Cut7 also generates outward force in an additive manner. This force-generating process collaborates with Ase1 to maintain microtubule bundling of anaphase B spindles and that Klp9 plays a role in this branch independently of its motility (bottom right). The motor-independent role of Klp9 requires the NLS and two coiled coil domains locating at the C-terminal non-motor region. Cut7 may not be involved in this microtubule crosslinking; or at least its role is less important compared with that played by Klp9.

Recently, it has become clear that fungal Kinesin-5s including Cut7 are bidirectional motors; they display either plus end-directed or minus end-directed motilities depending upon conditions (eg. the degree of motor crowding on the microtubule lattice)[63–65]. Under our experimental conditions, we did not detect a similar bi-directionality. It would be of interest to address where this difference stems from and explore the physiologies behind their distinct properties.

Dual roles of Kinesin-6 Klp9 in spindle elongation and microtubule bundling during anaphase B. We show that Klp9 does not require its motor activity to carry out essential functions in the absence of Ase1 (Fig. 3). Instead, it depends upon the two domains within the C-terminal non-motor region: two coiled coils and the NLS (Figs 4 and 5). It is of note that it remains established as to whether the sole role of this NLS lies in nuclear import activity or it has additional activity such as microtubule binding. Klp9 forms homotetramers like Cut7 (Fig. 1A,B)[37] and the analogous C-terminal coiled coils in Cut7 and other Kinesin-5 members are responsible for self-tetramerisation[66–68]. We envision that coiled coil-dependent homotetramers of Klp9 play a structural role in the bundling of antiparallel microtubules at the spindle midzone together with Ase1. To our knowledge, this is the first report on kinesin molecules that play a motor-independent role in microtubule crosslinking in a physiological context. Whether Kinesin-6 members in other species play an analogous role would be of great interest to be explored. Moreover, it is tempting to speculate that Klp9 is involved in the regulatory processes beyond simple sliding and crosslinking of microtubules; it may ensure proper anaphase B progression through regulating the elasticity and plasticity of microtubule overlapping zones as proposed for vertebrate Kinesin-5[69].

Roles of Kinesin-5 Cut7 during late mitosis. Using a newly isolated *cut7* ts allele, *cut7-122*, our analysis uncovered the crucial role of Cut7 as a motor in late mitosis. Spindle elongation rate in a single *cut7-122* mutant is reduced by 11% compared to wild type cells, while that in a *klp9*Δ strain drops by 49% and in a *cut7-122klp9*Δ double mutant, the reduction reaches 73% (Fig. 6E). As the *cut7-122* strain is most likely hypomorphic, not a complete loss of function, this degree of contribution from Cut7 to anaphase B spindle elongation is potentially underestimated. To address how these two motors collaborate with each other on the antiparallel microtubules, performing TIRFM[70] in the presence of individual proteins or a mixture of the two as a microtubule pair sliding assay would provide useful information.

Despite its slow velocity, we still detect spindle elongation in the *cut7-122klp9*Δ double mutant (retaining 27% activity compared to wild type cells). As aforementioned, although the Cut7-122 proteins are unlikely to have completely abolished motor activity, cells might still be capable of undergoing spindle elongation without kinesin-generated motor activities. This could be ascribable to the outward forces elicited by non-motor MAPs, including microtubule polymerisation and/or Ase1- and CLASP/Cls1-mediated microtubule bundling and stabilisation as previously pointed out[25,26].

Although the requirement of Cut7 for anaphase B spindle elongation has been established in this study, whether Cut7 plays another motor-independent role in microtubule bundling, analogous to Klp9, remains undetermined. We observed that *klp9* mutants which cannot form homotetramers are synthetically lethal with *ase1*Δ regardless of Cut7's presence (Fig. 5A). This raises the possibility that Cut7 may not be involved in microtubule crosslinking or at least its role is not as critical as that of Klp9. Thus, activities and/or properties of microtubule binding may not be identical between Cut7 and Klp9. Further cell biological and *in vitro* assays are required to clarify whether Cut7 is implicated in spindle integrity during anaphase B in a motor-independent manner.

Cell cycle-dependent cellular localisation of Kinesin-6 Klp9. We have identified a canonical NLS in the C-terminal region of Klp9 that is essential for its mitotic function. Klp9 constructs without a functional NLS could still be loaded onto the spindle midzone within the nucleus, though with reduced levels (Fig. 4A,B). Thus, it is likely that Klp9 is transported into the nucleus in a dual manner: one through its own NLS and the other perhaps through binding to another protein. Ase1, which acts together with Klp9 during anaphase B, might well be such a binding partner; however, two previous reports[37,45] as to whether Klp9 physically binds Ase1 are somewhat controversial. Hence, how Klp9 is localised to the mitotic nucleus in an NLS-independent manner remains undetermined. However, it is worth noting that despite the capability of its NLS-independent nuclear import during late mitosis, levels of Klp9 on spindles are insufficient to support the mitotic role of Klp9 (Fig. 4A). Thus, the NLS within the C-terminal domain of Klp9 is essential for Klp9 function.

Kinesin-5 and Kinesin-6 in spindle elongation in other species. The role of Kinesin-5 in bipolar spindle assembly, in particular during very early mitotic stages when the two centrosomes separate, is conserved across many eukaryotic species[71]. In addition, Kinesin-6 members ubiquitously participate in late mitotic events. Yet, the functional interplay between these two kinesins, if any, remains to be reported[10]. The results presented in the current study are the first to explore this notion. In budding yeast, Kinesin-5 Cin8 concentrates on central spindle microtubules during anaphase and plays a critical role in the maintenance of spindle pole separation[8,72]. However, this organism does not contain Kinesin-6 members. Instead, it has another Kinesin-5 Kip1, which collaborates with Cin8 in spindle elongation. It is likely that this yeast has developed a unique evolutionary strategy by which two different Kinesin-5 members compensate for the functions of Kinesin-6 in anaphase B spindle elongation. It is of note that a recent study showed that Kinesin-8 Kip3 acts in late mitosis together with Kip1[73].

In higher eukaryotes, multiple Kinesin-6 proteins play collaborative roles in spindle elongation during anaphase B coupled with cytokinesis. In *Drosophila melanogaster*, Kinesin-5 Klp61F and Kinesin-6 Subito work together in maintaining meiotic bipolar spindles[74]. Subito is known to be an important kinesin for mitotic spindle assembly as well. It would be of great interest to address whether and how the collaboration between Klp61F and Subito in spindle assembly extends into mitosis.

Materials and Methods

Strains, media and growth conditions. Strains used in this study are listed in Supplementary Table S1. Media, cultivation conditions, and manipulations were performed as previously described[75–77]. For most of the experiments, cells were grown in rich YE5S liquid media and on agar plates. Spot tests were carried out by spotting 5–10 μl of cells at a concentration of 2×10^7 cells/ml after 10-fold sequential dilutions onto rich YE5S plates. Plates were kept at various temperatures from 27 °C to 36 °C as appropriate.

Nucleic acids preparation and manipulation. DNA-manipulating enzymes were used as recommended by the manufacturers (New England Biolabs Inc. Ipswich, MA, U. S. A. and Takara Bio Inc., Shiga, Japan).

Construction of recombinant kinesins. To construct a full-length Klp9 expressing vector (pcDNA3.4/SpKlp9FL-EGFP-FLAG-His8), the full-length *klp9* cDNA was PCR amplified from a cDNA library (National BioResource Project, pTN-RC5) with a forward primer, ATGATACAGATTTTTCTGCGTGT and a reverse primer, AATTCATTAATATCGATATCAGTTG, and inserted into a modified pcDNA3.4 vector (pcDNA3.4/EGFP-FLAG-His8) via appropriate oligo nucleotide adaptors for the acceptor vector using the Gibson Assembly method. The resultant linker amino acid between SpKlp9 and EGFP is AAA (one-letter amino-acid code).

To construct Eg5-EGFP (pcDNA3.4/HsEg5FL-EGFP-FLAG-His8), the full-length human *Eg5* cDNA was amplified from a cDNA library constructed from HEK293 cells using the SV Total RNA Isolation System (Z3100, Promega Co. Fitchburg, WI, U. S. A.) and the SuperScript III First-Strand Synthesis System (18080-051, Invitrogen Co., Waltham, MA, U. S. A.). To construct kinesin-1-EGFP (pcDNA3.4/rk430-EGFP-FLAG-His8), the rat kinesin-1 fragment (1–430) was inserted into the modified pcDNA3.4 vector (pcDNA3.4/EGFP-FLAG-His8).

Expression and purification of proteins. We essentially followed procedures described previously[78]. The Expi293 Expression System (A14635, Invitrogen Co., Waltham, MA, U. S. A.) were used for transient expression of Klp9, Eg5 and kinesin-1 according to the manufacturer's instructions except that transfection was enhanced with PEI Max (24765-2, Polysciences Inc. Warrington, PA, U. S. A.) instead of the ExpiFectamine 293 Reagent. Cells from 1-L culture were used for two-step purification using Ni-IMAC and FLAG agarose. Protein concentration was determined by the Bradford assay using bovine serum albumin as a standard.

Preparation of fluorescently labelled microtubules. Tubulin was purified from pig brain using a high-molarity PIPES buffer (1 M PIPES-KOH pH 6.8, 20 mM EGTA, and 10 mM $MgCl_2$) as described previously[79]. Tubulin was labelled with Cy3 (PA23001, GE Healthcare) or ATTO 647N (AD 647N-31, ATTO-TEC). ATTO 647N-microtubules were polymerised by copolymerising labelled and unlabelled tubulin at a ratio of 1:5 for 30 min at 37 °C, and taxol-stabilised (T1912, Sigma-Aldrich St. Louis, MO, U. S. A.). Polarity-marked microtubules were prepared as described previously[80].

Quantification of fluorescence signal intensities of purified proteins on a glass surface. Flow chambers were assembled from two coverslips (18 × 18 mm and 24 × 32 mm, Matsunami Glass Ltd., Osaka, Japan) with two slivers of Parafilm as a spacer. The coverslips were heat-sealed on a 98 °C hot plate. GFP-tagged proteins were appropriately diluted in HME buffer (20 mM HEPES pH 7.4 adjusted with NaOH, 2 mM $MgCl_2$ and 1 mM EGTA), and then perfused into a flow chamber. After checking the adsorption of GFP-labelled kinesins to the glass surface, the flow chamber was washed with HME buffer supplemented with 2 mM dithiothreitol, 25 mM glucose, 21.3 U/ml glucose oxidase and 800 U/ml catalase.

Fluorescence spots were imaged using an objective-type TIRFM based on Ti-E (Nikon) equipped with a 488-nm laser (488-75CDRH, Coherent Inc., Santa Clara, CA, U. S. A.) and a ×60/NA1.49 oil immersion objective lens (CFI Apo TIRF 60xH, Nikon Inc., Tokyo, Japan) at 24 ± 1 °C. Images were magnified by 2.5× TV-adaptor (MQD42120, Nikon Inc., Tokyo, Japan) and projected onto an EMCCD detector (C9100-13, Hamamatsu Photonics K.K., Shizuoka, Japan). The camera was controlled by the Micro-manager software ver. 1.4.2243. Photobleaching behaviour of Klp9-EGFP was analysed by summing intensities from a 9 × 9-pixel region and subtracting the mean intensity of 9–10 regions around each fluorescence spot as a background intensity after four-frame rolling averaging using the Running Z projector plugin for ImageJ. To obtain the intensity profile of GFP-labelled kinesins adsorbed to a glass surface, the TrackMate plugin ver. 3.5.1 for Fiji was used to automatically detect and quantify the intensities of fluorescence spots. The DoG (Difference of Gaussian) detector with an estimated diameter of 9 pixels and a threshold value of 3 were used. Background intensity was measured at 9–10 random background regions in the field of view and subtracted from individual intensities of fluorescence spots.

Microtubule gliding assay. A flow chamber was first filled with 7 μl of antibody to penta-His (#34660, Qiagen; 1/10 dilution) and incubated for 5 min. The chamber was next coated with 1% w/v Pluronic F-127 (P2443, Sigma-Aldrich, St. Louis, MO, U. S. A.) for 5 min and blocked with 0.6–0.7 mg/ml casein (#07319-82, Nacalai Tesque Inc., Kyoto, Japan) in BRB80 buffer (80 mM PIPES-KOH pH 6.8, 1 mM EGTA and 1 mM $MgCl_2$). Then 40 μg/ml Klp9 solution in BRB80 buffer was perfused and incubated for 5 min. After washing with 21 μl of BRB80 buffer including 0.6–0.7 mg/ml casein, the final solution containing the fluorescently labelled polarity-marked microtubules, 0.218 mg/ml glucose oxidase (G2133, Sigma-Aldrich, St. Louis, MO, U. S. A.), 0.04 mg/ml catalase (219001, Calbiochem Co., South San Francisco, CA, U. S. A.), 25 mM glucose, ~0.7 mg/ml casein, 2 mM DTT, 10 μM paclitaxel and 1 mM ATP in BRB80 buffer, was introduced into the flow chamber. After a 15 s incubation, final solution without microtubules was perfused into the flow chamber.

Microtubule gliding was imaged using the same setup as intensity measurement described above except that a 532-nm laser (CDPS532S-020, JDS Uniphase Co., Milpitas, CA, U. S. A.) was used for TIRF illumination. The position of the filament was determined manually by mouse clicking on the tip of the filament in the standalone custom software (Mark2 ver. 2.6) and tracked typically every 10 s. Microtubules that glided for at least 10 s were included in velocity measurement. After the distance travelled were plotted against time, velocities were determined by the slope calculated from the linear regression of each trace.

Single molecule motility assay. We imaged single-molecule behaviour of Klp9 as previously described[78]. To immobilise microtubules, a dimethyldichlorosilane-treated flow chamber was incubated with 1:10 diluted anti-tubulin antibody (66031-1-Ig, Proteintech Group Inc., Chicago, IL, U. S. A.) in BRB80 buffer for 5 min and blocked with 1% w/v Pluronic F-127 in BRB80 buffer. After washing with 0.6–0.7 mg/ml casein in BRB80 buffer, ATTO 647N-labelled microtubules in BRB80 buffer was perfused and incubated for 5 min. After further washing with 0.6–0.7 mg/ml casein, the final solution containing 0.3 nM Klp9-EGFP, 20 mM HEPES pH 7.4 adjusted with NaOH, 2 mM $MgCl_2$, 1 mM EGTA, 10 mM K-acetate, 10 μM paclitaxel, 0.7 mg/ml casein, 2 mM dithiothreitol, 25 mM glucose, 21.3 U/ml glucose oxidase, 800 U/ml catalase and 1 mM ATP was added to the flow chamber. To confirm the polarity of the microtubules, the chamber was perfused with kinesin-1 labelled with Alexa546 after measurement.

Single-molecule behaviour of GFP-kinesins was imaged using the same setup as intensity measurement described above except that a 632.8-nm laser (30991, Research Electro Optics Inc., Boulder, CO, U. S.A.) was used along with a 488-nm laser (488-75CDRH, Coherent, Inc., Santa Clara, CA, U. S. A.) for TIRF illumination. The image framerate was 100 ms per frame. The custom software (Mark2 ver.2.6) was used to manually pick fluorescence spots and to determine their sub-pixel positions by using automated two-dimensional Gaussian fitting algorithm. All fluorescence spots that moved on a given microtubule were picked but ones that disappeared within 1.2 s or travelled a distance of less than 200 nm were excluded. After the position of the fluorescence spots along the microtubule were plotted against time, velocities were determined by the slope calculated from the linear regression of each trace.

Strain construction, gene deletion and epitope tagging. A simple PCR-based strategy[76,77] was used for complete gene deletion and epitope tagging in the C terminus, thereby all the tagged proteins being expressed under their own endogenous promoter.

Isolation of *cut7* temperature-sensitive mutants in the *klp9*Δ background. The *cut7* ts mutants were constructed by PCR-based random mutagenesis. The GFP epitope tag and G418-resistance marker gene cassette (*kanR*) were first inserted into the 3′ flanking region of the *cut7* gene (*cut7-GFP-kanR*). The *cut7-GFP-kanR* fragment purified from this strain was amplified/mutagenised with PCR using *TaKaRa EX* taq polymerase (Takara Bio Inc., Shiga, Japan) and transformed into a *klp9*Δ strain (deleted by *hphR*). G418 (and Hygromycin B)-resistant colonies were picked up and backcrossed with a wild type strain. After confirming co-segregation between G418/Hygromycin B-resistance and the ts phenotype, nucleotide sequencing was performed to determine the mutated sites within the *cut7* gene of these mutants.

Fluorescence imaging of live cells. Procedures previously described[24,81] were essentially followed. Fluorescence imaging experiments were performed with a DeltaVision Elite microscope system (GE Healthcare, Chicago, IL, U. S. A.), which is a wide-field inverted epifluorescence microscope (IX71; Olympus, Tokyo, Japan) equipped with a PLAPON 60× 1.40 NA oil objective lens (Olympus, Tokyo, Japan). Fluorescence images were captured by a charge-coupled device camera (CoolSNAP HQ2; Photometrics, Tucson, AZ, U. S. A.) and the softWoRx 6.5.2 software (GE Healthcare, Chicago, IL). Live cells were imaged in a glass-bottomed culture dish (MatTek Corporation, Ashland, MA, U. S. A.) coated with soybean lectin (L1395, Sigma-Aldrich, St. Louis, MO, U. S. A.) and incubated at 27 °C for most of the strains or at 36 °C for the ts mutants. For ts mutants, cells were cultured in rich YE5S media until mid–log phase at 27 °C and subsequently shifted to the restrictive temperature of 36 °C for further culture until observation. To keep cultures at the proper temperature, cell culture dishes were mounted in a temperature-controlled chamber (Air Therm SMT; World Precision Instruments Inc., Sarasota, FL, U. S. A.). Images of 14–16 sections were taken along the z-axis at 0.2-μm intervals at each time point. After deconvolution, projection images of maximum intensity were obtained. Captured images were processed with Photoshop CS6 (version 13.0; Adobe, San Jose, CA. U. S. A.).

Quantification of fluorescence signal intensities in cells. For quantification of signal intensities of Klp9-GFP located at the spindle midzone during anaphase B, 14–16 sections were taken along the z-axis at 0.2-μm intervals. After deconvolution and projection images of maximum intensity, a 20 × 20–pixel (2.15-μm square) region of interest (ROI) with maximum sum intensity was determined. After subtracting the mean intensity of three regions around each ROI as background intensities, values of the maximum sum intensities were used for statistical data analysis.

Statistical analysis. The significance of differences in different strains was determined by the two-tailed unpaired Student's *t*-test. All the experiments were repeated at least twice. Sample numbers used for statistical analysis were presented in the corresponding figures and/or legends. Asterisks shown in the figures indicate the p-values as follows: ****$P < 0.0001$. $P < 0.05$ was considered to be statistically significant.

References

1. Godinho, S. A. & Pellman, D. Causes and consequences of centrosome abnormalities in cancer. *Philos Trans R Soc Lond B Biol Sci* **369**, https://doi.org/10.1098/rstb.2013.0467 (2014).
2. Reber, S. & Hyman, A. A. Emergent properties of the metaphase spindle. *Cold Spring Harb Perspect Biol* **7**, a015784, https://doi.org/10.1101/cshperspect.a015784 (2015).
3. Blangy, A. *et al*. Phosphorylation by $p34^{cdc2}$ regulates spindle association of human Eg5, a kinesin-related motor essential for bipolar spindle formation *in vivo*. *Cell* **83**, 1159–1169 (1995).
4. Enos, A. P. & Morris, N. R. Mutation of a gene that encodes a kinesin-like protein blocks nuclear division in *A. nidulans*. *Cell* **60**, 1019–1027 (1990).
5. Hagan, I. & Yanagida, M. Novel potential mitotic motor protein encoded by the fission yeast $cut7^{+}$ gene. *Nature* **347**, 563–566, https://doi.org/10.1038/347563a0 (1990).
6. Heck, M. M. *et al*. The kinesin-like protein KLP61F is essential for mitosis in *Drosophila*. *J Cell Biol* **123**, 665–679 (1993).
7. Le Guellec, R., Paris, J., Couturier, A., Roghi, C. & Philippe, M. Cloning by differential screening of a *Xenopus* cDNA that encodes a kinesin-related protein. *Mol Cell Biol* **11**, 3395–3398 (1991).
8. Hoyt, M. A., He, L., Loo, K. K. & Saunders, W. S. Two *Saccharomyces cerevisiae* kinesin-related gene products required for mitotic spindle assembly. *J Cell Biol* **118**, 109–120 (1992).
9. Roof, D. M., Meluh, P. B. & Rose, M. D. Kinesin-related proteins required for assembly of the mitotic spindle. *J Cell Biol* **118**, 95–108 (1992).
10. Yount, A. L., Zong, H. & Walczak, C. E. Regulatory mechanisms that control mitotic kinesins. *Exp Cell Res* **334**, 70–77, https://doi.org/10.1016/j.yexcr.2014.12.015 (2015).
11. Tanenbaum, M. E. & Medema, R. H. Mechanisms of centrosome separation and bipolar spindle assembly. *Dev. Cell* **19**, 797–806, https://doi.org/10.1016/j.devcel.2010.11.011 (2010).
12. Sharp, D. J., Rogers, G. C. & Scholey, J. M. Microtubule motors in mitosis. *Nature* **407**, 41–47, https://doi.org/10.1038/35024000 (2000).
13. Kapitein, L. C. *et al*. The bipolar mitotic kinesin Eg5 moves on both microtubules that it crosslinks. *Nature* **435**, 114–118, https://doi.org/10.1038/nature03503 (2005).
14. Kashina, A. S. *et al*. A bipolar kinesin. *Nature* **379**, 270–272, https://doi.org/10.1038/379270a0 (1996).
15. Civelekoglu-Scholey, G., Tao, L., Brust-Mascher, I., Wollman, R. & Scholey, J. M. Prometaphase spindle maintenance by an antagonistic motor-dependent force balance made robust by a disassembling lamin-B envelope. *J Cell Biol* **188**, 49–68, https://doi.org/10.1083/jcb.200908150 (2010).
16. Mountain, V. *et al*. The kinesin-related protein, HSET, opposes the activity of Eg5 and cross-links microtubules in the mammalian mitotic spindle. *J Cell Biol* **147**, 351–366 (1999).
17. O'Connell, M. J., Meluh, P. B., Rose, M. D. & Morris, N. R. Suppression of the *bimC4* mitotic spindle defect by deletion of *klpA*, a gene encoding a KAR3-related kinesin-like protein in *Aspergillus nidulans*. *J Cell Biol* **120**, 153–162 (1993).
18. Pidoux, A. L., LeDizet, M. & Cande, W. Z. Fission yeast pkl1 is a kinesis-related protein involved in mitotic spindle function. *Mol. Biol. Cell* **7**, 1639–1655 (1996).
19. Troxell, C. L. *et al*. $pkl1^{+}$: and $klp2^{+}$: two kinesins of the Kar3 subfamily in fission yeast perform different functions in both mitosis and meiosis. *Mol Biol Cell* **12**, 3476–3488, https://doi.org/10.1091/mbc.12.11.3476 (2001).
20. Saunders, W., Lengyel, V. & Hoyt, M. A. Mitotic spindle function in *Saccharomyces cerevisiae* requires a balance between different types of kinesin-related motors. *Mol Biol Cell* **8**, 1025–1033 (1997).
21. Sharp, D. J., Yu, K. R., Sisson, J. C., Sullivan, W. & Scholey, J. M. Antagonistic microtubule-sliding motors position mitotic centrosomes in *Drosophila* early embryos. *Nat Cell Biol* **1**, 51–54, https://doi.org/10.1038/9025 (1999).
22. Tao, L. *et al*. A homotetrameric kinesin-5, KLP61F, bundles microtubules and antagonizes Ncd in motility assays. *Curr Biol* **16**, 2293–2302, https://doi.org/10.1016/j.cub.2006.09.064 (2006).
23. Walczak, C. E., Vernos, I., Mitchison, T. J., Karsenti, E. & Heald, R. A model for the proposed roles of different microtubule-based motor proteins in establishing spindle bipolarity. *Curr Biol* **8**, 903–913 (1998).
24. Yukawa, M., Yamada, Y., Yamauchi, T. & Toda, T. Two spatially distinct kinesin-14 proteins, Pkl1 and Klp2, generate collaborative inward forces against kinesin-5 Cut7 in *S. pombe*. *J Cell Sci* **131**, 1–11, https://doi.org/10.1242/jcs.210740 (2018).

25. Rincon, S. A. *et al.* Kinesin-5-independent mitotic spindle assembly requires the antiparallel microtubule crosslinker Ase1 in fission yeast. *Nat Commun* **8**, 15286, https://doi.org/10.1038/ncomms15286 (2017).
26. Yukawa, M. *et al.* A microtubule polymerase cooperates with the kinesin-6 motor and a microtubule cross-linker to promote bipolar spindle assembly in the absence of kinesin-5 and kinesin-14 in fission yeast. *Mol Biol Cell* **28**, 3647–3659, https://doi.org/10.1091/mbc.E17-08-0497 (2017).
27. Syrovatkina, V. & Tran, P. T. Loss of kinesin-14 results in aneuploidy via kinesin-5-dependent microtubule protrusions leading to chromosome cut. *Nat Commun* **6**, 7322, https://doi.org/10.1038/ncomms8322 (2015).
28. Olmsted, Z. T., Colliver, A. G., Riehlman, T. D. & Paluh, J. L. Kinesin-14 and kinesin-5 antagonistically regulate microtubule nucleation by γ-TuRC in yeast and human cells. *Nat Commun* **5**, 5339, https://doi.org/10.1038/ncomms6339 (2014).
29. Rodriguez, A. S. *et al.* Protein complexes at the microtubule organizing center regulate bipolar spindle assembly. *Cell Cycle* **7**, 1246–1253, https://doi.org/10.4161/cc.7.9.5808 (2008).
30. Verhey, K. J. & Hammond, J. W. Traffic control: regulation of kinesin motors. *Nat Rev Mol Cell Biol* **10**, 765–777, https://doi.org/10.1038/nrm2782 (2009).
31. Goshima, G. & Scholey, J. M. Control of mitotic spindle length. *Annu. Rev. Cell Dev. Biol.* **26**, 21–57, https://doi.org/10.1146/annurev-cellbio-100109-104006 (2010).
32. Lawrence, C. J. *et al.* A standardized kinesin nomenclature. *J Cell Biol* **167**, 19–22, https://doi.org/10.1083/jcb.200408113 (2004).
33. Hirokawa, N., Noda, Y., Tanaka, Y. & Niwa, S. Kinesin superfamily motor proteins and intracellular transport. *Nat Rev Mol Cell Biol* **10**, 682–696, https://doi.org/10.1038/nrm2774 (2009).
34. Abaza, A. *et al.* M phase phosphoprotein 1 is a human plus-end-directed kinesin-related protein required for cytokinesis. *J Biol Chem* **278**, 27844–27852, https://doi.org/10.1074/jbc.M304522200 (2003).
35. Adams, R. R., Tavares, A. A., Salzberg, A., Bellen, H. J. & Glover, D. M. *pavarotti* encodes a kinesin-like protein required to organize the central spindle and contractile ring for cytokinesis. *Genes Dev* **12**, 1483–1494 (1998).
36. Cesario, J. M. *et al.* Kinesin 6 family member Subito participates in mitotic spindle assembly and interacts with mitotic regulators. *J Cell Sci* **119**, 4770–4780, https://doi.org/10.1242/jcs.03235 (2006).
37. Fu, C. *et al.* Phospho-regulated interaction between kinesin-6 Klp9p and microtubule bundler Ase1p promotes spindle elongation. *Dev Cell* **17**, 257–267, https://doi.org/10.1016/j.devcel.2009.06.012 (2009).
38. Hill, E., Clarke, M. & Barr, F. A. The Rab6-binding kinesin, Rab6-KIFL, is required for cytokinesis. *EMBO J* **19**, 5711–5719, https://doi.org/10.1093/emboj/19.21.5711 (2000).
39. Nislow, C., Lombillo, V. A., Kuriyama, R. & McIntosh, J. R. A plus-end-directed motor enzyme that moves antiparallel microtubules *in vitro* localizes to the interzone of mitotic spindles. *Nature* **359**, 543–547, https://doi.org/10.1038/359543a0 (1992).
40. Raich, W. B., Moran, A. N., Rothman, J. H. & Hardin, J. Cytokinesis and midzone microtubule organization in *Caenorhabditis elegans* require the kinesin-like protein ZEN-4. *Mol Biol Cell* **9**, 2037–2049 (1998).
41. Zhu, C. *et al.* Functional analysis of human microtubule-based motor proteins, the kinesins and dyneins, in mitosis/cytokinesis using RNA interference. *Mol Biol Cell* **16**, 3187–3199, https://doi.org/10.1091/mbc.e05-02-0167 (2005).
42. Gruneberg, U., Neef, R., Honda, R., Nigg, E. A. & Barr, F. A. Relocation of Aurora B from centromeres to the central spindle at the metaphase to anaphase transition requires MKlp2. *J Cell Biol* **166**, 167–172, https://doi.org/10.1083/jcb.200403084 (2004).
43. Janisch, K. M., McNeely, K. C., Dardick, J. M., Lim, S. H. & Dwyer, N. D. Kinesin-6 KIF20B is required for efficient cytokinetic furrowing and timely abscission in human cells. *Mol Biol Cell* **29**, 166–179, https://doi.org/10.1091/mbc.E17-08-0495 (2018).
44. Jang, J. K., Rahman, T. & McKim, K. S. The kinesinlike protein Subito contributes to central spindle assembly and organization of the meiotic spindle in Drosophila oocytes. *Mol Biol Cell* **16**, 4684–4694, https://doi.org/10.1091/mbc.e04-11-0964 (2005).
45. Meadows, J. C. *et al.* Identification of a Sgo2-dependent but Mad2-independent pathway controlling anaphase onset in fission yeast. *Cell Rep* **18**, 1422–1433, https://doi.org/10.1016/j.celrep.2017.01.032 (2017).
46. White, E. A. & Glotzer, M. Centralspindlin: at the heart of cytokinesis. *Cytoskeleton (Hoboken)* **69**, 882–892, https://doi.org/10.1002/cm.21065 (2012).
47. Bieling, P., Telley, I. A. & Surrey, T. A minimal midzone protein module controls formation and length of antiparallel microtubule overlaps. *Cell* **142**, 420–432, https://doi.org/10.1016/j.cell.2010.06.033 (2010).
48. Subramanian, R. *et al.* Insights into antiparallel microtubule crosslinking by PRC1, a conserved nonmotor microtubule binding protein. *Cell* **142**, 433–443, https://doi.org/10.1016/j.cell.2010.07.012 (2010).
49. Janson, M. E. *et al.* Crosslinkers and motors organize dynamic microtubules to form stable bipolar arrays in fission yeast. *Cell* **128**, 357–368, https://doi.org/10.1016/j.cell.2006.12.030 (2007).
50. Loiodice, I. *et al.* Ase1p organizes antiparallel microtubule arrays during interphase and mitosis in fission yeast. *Mol Biol Cell* **16**, 1756–1768, https://doi.org/10.1091/mbc.e04-10-0899 (2005).
51. Yamashita, A., Sato, M., Fujita, A., Yamamoto, M. & Toda, T. The roles of fission yeast ase1 in mitotic cell division, meiotic nuclear oscillation, and cytokinesis checkpoint signaling. *Mol Biol Cell* **16**, 1378–1395, https://doi.org/10.1091/mbc.E04-10-0859 (2005).
52. Weinger, J. S., Qiu, M., Yang, G. & Kapoor, T. M. A nonmotor microtubule binding site in kinesin-5 is required for filament crosslinking and sliding. *Curr Biol* **21**, 154–160, https://doi.org/10.1016/j.cub.2010.12.038 (2011).
53. Kapitein, L. C. *et al.* Microtubule-driven multimerization recruits ase1p onto overlapping microtubules. *Curr Biol* **18**, 1713–1717, https://doi.org/10.1016/j.cub.2008.09.046 (2008).
54. Toda, T., Adachi, Y., Hiraoka, Y. & Yanagida, M. Identification of the pleiotropic cell division cycle gene *NDA2* as one of two different α-tubulin genes in *Schizosaccharomyces pombe*. *Cell* **37**, 233–242, doi:0092-8674(84)90319-2 [pii] (1984).
55. Meadows, J. C. & Millar, J. Latrunculin A delays anaphase onset in fission yeast by disrupting an Ase1-independent pathway controlling mitotic spindle stability. *Mol Biol Cell* **19**, 3713–3723, https://doi.org/10.1091/mbc.E08-02-0164 (2008).
56. Kalderon, D., Roberts, B. L., Richardson, W. D. & Smith, A. E. A short amino acid sequence able to specify nuclear location. *Cell* **39**, 499–509 (1984).
57. Kruger, L. K., Sanchez, J. L., Paoletti, A. & Tran, P. T. Kinesin-6 regulates cell-size-dependent spindle elongation velocity to keep mitosis duration constant in fission yeast. *eLife* **8**, e42182, https://doi.org/10.7554/eLife.42182 (2019).
58. Hagan, I. & Yanagida, M. Kinesin-related cut7 protein associates with mitotic and meiotic spindles in fission yeast. *Nature* **356**, 74–76, https://doi.org/10.1038/356074a0 (1992).
59. Chang, L. & Gould, K. L. Sid4p is required to localize components of the septation initiation pathway to the spindle pole body in fission yeast. *Proc Natl Acad Sci USA* **97**, 5249–5254, https://doi.org/10.1073/pnas.97.10.5249 (2000).
60. Syrovatkina, V., Fu, C. & Tran, P. T. Antagonistic spindle motors and MAPs regulate metaphase spindle length and chromosome segregation. *Curr Biol* **23**, 2423–2429, https://doi.org/10.1016/j.cub.2013.10.023 (2013).
61. Kwok, B. H., Yang, J. G. & Kapoor, T. M. The rate of bipolar spindle assembly depends on the microtubule-gliding velocity of the mitotic kinesin Eg5. *Curr Biol* **14**, 1783–1788, https://doi.org/10.1016/j.cub.2004.09.052 (2004).
62. Gerson-Gurwitz, A. *et al.* Directionality of individual kinesin-5 Cin8 motors is modulated by loop 8, ionic strength and microtubule geometry. *EMBO J* **30**, 4942–4954, https://doi.org/10.1038/emboj.2011.403 (2011).
63. Edamatsu, M. Bidirectional motility of the fission yeast kinesin-5, Cut7. *Biochem. Biophys. Res. Commun.* **446**, 231–234, https://doi.org/10.1016/j.bbrc.2014.02.106 (2014).
64. Britto, M. *et al. Schizosaccharomyces pombe* kinesin-5 switches direction using a steric blocking mechanism. *Proc Natl Acad Sci USA* **113**, E7483–E7489, https://doi.org/10.1073/pnas.1611581113 (2016).

65. Singh, S. K., Pandey, H., Al-Bassam, J. & Gheber, L. Bidirectional motility of kinesin-5 motor proteins: structural determinants, cumulative functions and physiological roles. *Cell Mol Life Sci* **75**, 1757–1771, https://doi.org/10.1007/s00018-018-2754-7 (2018).
66. Akera, T., Goto, Y., Sato, M., Yamamoto, M. & Watanabe, Y. Mad1 promotes chromosome congression by anchoring a kinesin motor to the kinetochore. *Nat Cell Biol* **17**, 1124–1133, https://doi.org/10.1038/ncb3219 (2015).
67. Acar, S. *et al*. The bipolar assembly domain of the mitotic motor kinesin-5. *Nat Commun* **4**, 1343, https://doi.org/10.1038/ncomms2348 (2013).
68. Scholey, J. E., Nithianantham, S., Scholey, J. M. & Al-Bassam, J. Structural basis for the assembly of the mitotic motor Kinesin-5 into bipolar tetramers. *eLife* **3**, e02217, https://doi.org/10.7554/eLife.02217 (2014).
69. Shimamoto, Y., Forth, S. & Kapoor, T. M. Measuring pushing and braking forces generated by ensembles of kinesin-5 crosslinking two microtubules. *Dev Cell* **34**, 669–681, https://doi.org/10.1016/j.devcel.2015.08.017 (2015).
70. Bieling, P., Telley, I. A., Hentrich, C., Piehler, J. & Surrey, T. Fluorescence microscopy assays on chemically functionalized surfaces for quantitative imaging of microtubule, motor, and +TIP dynamics. *Methods Cell Biol* **95**, 555–580, https://doi.org/10.1016/S0091-679X(10)95028-0 (2010).
71. Mann, B. J. & Wadsworth, P. Kinesin-5 Regulation and Function in Mitosis. *Trends Cell Biol* **29**, 66–79, https://doi.org/10.1016/j.tcb.2018.08.004 (2019).
72. Straight, A. F., Sedat, J. W. & Murray, A. W. Time-lapse microscopy reveals unique roles for kinesins during anaphase in budding yeast. *J Cell Biol* **143**, 687–694 (1998).
73. Ibarlucea-Benitez, I., Ferro, L. S., Drubin, D. G. & Barnes, G. Kinesins relocalize the chromosomal passenger complex to the midzone for spindle disassembly. *J Cell Biol* **217**, 1687–1700, https://doi.org/10.1083/jcb.201708114 (2018).
74. Radford, S. J., Go, A. M. & McKim, K. S. Cooperation between kinesin motors promotes spindle symmetry and chromosome organization in oocytes. *Genetics* **205**, 517–527, https://doi.org/10.1534/genetics.116.194647 (2017).
75. Moreno, S., Klar, A. & Nurse, P. Molecular genetic analysis of fission yeast *Schizosaccharomyces pombe*. *Methods Enzymol* **194**, 795–823 (1991).
76. Bahler, J. *et al*. Heterologous modules for efficient and versatile PCR-based gene targeting in *Schizosaccharomyces pombe*. *Yeast* **14**, 943–951, 10.1002/(SICI)1097-0061(199807)14:10<943::AID-YEA292>3.0.CO;2-Y (1998).
77. Sato, M., Dhut, S. & Toda, T. New drug-resistant cassettes for gene disruption and epitope tagging in *Schizosaccharomyces pombe*. *Yeast* **22**, 583–591, https://doi.org/10.1002/yea.1233 (2005).
78. Torisawa, T. *et al*. Autoinhibition and cooperative activation mechanisms of cytoplasmic dynein. *Nat Cell Biol* **16**, 1118–1124, https://doi.org/10.1038/ncb3048 (2014).
79. Castoldi, M. & Popov, A. V. Purification of brain tubulin through two cycles of polymerization-depolymerization in a high-molarity buffer. *Protein expression and purification* **32**, 83–88, https://doi.org/10.1016/S1046-5928(03)00218-3 (2003).
80. Furuta, A. *et al*. Creating biomolecular motors based on dynein and actin-binding proteins. *Nature nanotechnology* **12**, 233–237, https://doi.org/10.1038/nnano.2016.238 (2017).
81. Yukawa, M., Yamada, Y. & Toda, T. Suppressor analysis uncovers that MAPs and microtubule dynamics balance with the Cut7/Kinesin-5 motor for mitotic spindle assembly in Schizosaccharomyces pombe. *G3 (Bethesda)* **9**, 269–280, https://doi.org/10.1534/g3.118.200896 (2019).

Acknowledgements

We are grateful to Paul Nurse, Iain Hagan, Jonathan Millar and J. Richard McIntosh for providing us with the strains used in this study. We thank Maki Yoshio for technical assistance and Kylie Pan for critical reading of the manuscript and useful suggestions. This work was supported by the Japan Society for the Promotion of Science (JSPS) (KAKENHI Scientific Research (A) 16H02503 to T.T., a Challenging Exploratory Research grant 16K14672 to T.T., Scientific Research (C) 16K07694 to M.Y., Scientific Research (C) 15KT0155 to K.F. and Grant-in-Aid for Scientific Research on Innovative Areas 18H05420 to K.F.), the Naito Foundation (T.T.) and the Uehara Memorial Foundation (T.T.).

Author Contributions

M.Y., K.F. and T.T. designed experiments. M.Y., K.F. M.O. and Y.T. performed experiments and analysed the data. T.T. organised a whole project. M.Y., K.F. and T.T. wrote the manuscript and M.O. and Y.T. made suggestions.

Additional Information

Supplementary information accompanies this paper at https://doi.org/10.1038/s41598-019-43774-7.

Competing Interests: The authors declare no competing interests.

Publisher's note: Springer Nature remains neutral with regard to jurisdictional claims in published maps and institutional affiliations.